

# Domain growth and surface roughening in Monte Carlo simulations of $A_{0.5}B_{0.5}$ film growth

Y. Shim and D. P. Landau

*Center for Simulational Physics, University of Georgia, Athens, Georgia 30602*

S. Pal

*104 Davey Laboratory, Department of Physics, The Pennsylvania State University, University Park, Pennsylvania, 16802*

(Received 23 June 1998)

Using Monte Carlo simulations of a simple model of  $A_{0.5}B_{0.5}$  film growth in 2+1 dimensions, we have calculated domain size, long-range order in each layer  $l$ , and surface fluctuations to examine the dynamic relation between surface-induced domain growth and growth-induced surface roughening. At early stages, small clusters of ordered domains grow due to short-range order fluctuations and then coalesce. A partially ordered layer acts as a template for further ordering in the next layer. At late times specific patterns of the domains emerge by coarsening processes. The mean square domain size  $R^2(l)$  shows a linear dependence on the layer number  $l$  for small  $l$  and saturates after  $l_s \sim L^{z_R}$  with domain growth exponent  $z_R = 2.02$ . In the asymptotic regime, the final morphology of the film is determined by the Laplacian term  $\nu \nabla^2 h$  in the continuum growth equation with roughness exponent  $\zeta = 0$  and dynamic exponent  $z = 2$ .

[S1063-651X(98)05512-3]

PACS number(s): 68.55.-a, 05.40.+j, 64.60.Cn, 05.70.Ln

## I. INTRODUCTION

There have been tremendous efforts made to understand growth-induced surface roughening and the underlying mechanisms of thin film growth by experiments and simulations [1,2]. From the point of view of simulation, simple discrete models of homoepitaxial film growth have been used most often, primarily to study intermediate- and long-time behavior of surface fluctuations, structure factors, and height-height correlations. Phenomenological continuum growth equations have been also derived from symmetry arguments and analyzed by renormalization group methods or numerical calculations; however, detailed mechanisms of  $A_x B_{1-x}$  film growth and the consequences of surface roughening processes are less well understood. Several groups have recently reported experimental observations of atomic ordering in alloy films of  $\text{Si}_{1-x}\text{Ge}_x$  [3],  $\text{Al}_x\text{Ga}_{1-x}\text{As}$  [4],  $\text{Ga}_x\text{In}_{1-x}\text{As}$  [5],  $\text{Ga}_x\text{In}_{1-x}\text{P}$  [6,7], etc., grown by epitaxial techniques. The degree of long-range order observed in the experiments is strongly affected by the properties of materials used and epitaxial conditions like surface temperature [3,8], growth rate [9], etc.

The observed ordering in  $\text{Si}_{1-x}\text{Ge}_x$  alloys [3] and at Si/Ge interfaces [10] is related to a kinetic growth process due to stresses at the growing surface and is then buried as the films grow. The growth of  $\text{Ga}_x\text{In}_{1-x}\text{P}$  alloys on GaAs substrates [6] shows that ordered domains start from the substrate and broaden as the films grow. Experiments indicate that ordering takes place near the surface exposed to the incoming particle-beam flux and show that the presence of long-range order (LRO) is mainly due to surface phenomena and cannot be explained by bulk or equilibrium properties. The ordering is a metastable state which is irreversibly destroyed by annealing although it is sustained up to a rather high temperature if bulk diffusion is negligible [3].

One interesting question is how atomic ordering in metallic alloys [11,12] and compound semiconductors [3-5,8,10]

is related to the surface roughening process during film growth. Recent experiments provided valuable information about the relationship between nonequilibrium surface morphology and ordering; in  $\text{Si}_x\text{Ge}_{1-x}$  [13] it is related to a Stranski-Krastanov growth mode, and in GaInP [14] it is linked to large steps formed by step bunching. A kinetic mean field calculation [15,16] [studying quasi-layer-by-layer growth and three-dimensional (3D) growth due to infinite step barriers at the step edge] also shows that the morphology of the films affects the evolution of the LRO. The scaling result of surface roughness in the growth of  $\text{Si}_{1-x}\text{Ge}_x$  on Si [17] indicates that at large length scales surface morphology shows Edwards-Wilkinson (EW) [18] behavior.

In this paper we report the results of the surface-induced domain growth and the growth-induced surface roughening for a simple model of binary alloy films grown by molecular-beam epitaxy (MBE) simulations. First of all, we mention that we do not attempt to include full complexity but deal with a rather simple model which will exhibit essential features of the system. In Sec. II we provide the background including the dynamic scaling theories of domain growth and surface roughening, and then we introduce our model and method in Sec. III. In Sec. IV the evolution and scaling behaviors of domain size and LRO are presented as a function of a layer number  $l$  after the LRO reaches its steady state. We present and discuss the scaling results of the interfacial width and the corresponding structure factor in Sec. IV. Finally, in Sec. V we conclude.

## II. BACKGROUND

### A. Domain growth

The formation of ordered domains, clusters, and droplets at early and late times has been a hot topic in nonequilibrium statistical physics. A theoretical description of pattern formation for the case of a nonconserved order parameter (NCOP)

is known as model A [19]. This is described by a Langevin equation for a one-component order parameter field  $\psi(\mathbf{r}, t)$ ,

$$\frac{\partial \psi(\mathbf{r}, t)}{\partial t} = -\Gamma \frac{\delta F}{\delta \psi(\mathbf{r}, t)} + \eta_0(\mathbf{r}, t), \quad (1)$$

with mobility  $\Gamma$  and a coarse-grained free energy  $F$  which is a functional of the local order parameter and has the Ginzburg-Landau form

$$F = \int d\mathbf{r} \left[ V(\psi) + \frac{\kappa_0}{2} (\nabla \psi)^2 \right], \quad (2)$$

with  $V(\psi) = \frac{1}{2} r_0 \psi^2 + \frac{1}{4} u_0 \psi^4$  in which  $u_0 > 0$ ,  $r_0 < 0$ , and  $\kappa_0 (> 0)$  is a constant related to the range of interaction. In a single disordered phase,  $V(\psi)$  has a stable, single-well structure with  $V(\psi) \approx \frac{1}{2} r_s \psi^2$  ( $r_s > 0$ ), and in the two-phase region ( $r_o < 0$ ),  $V(\psi)$  has a double-well structure. In Eq. (1),  $\eta_0(\mathbf{r}, t)$  is the stochastic white noise assumed to be  $\delta$  correlated in both space and time:

$$\langle \eta_0(\mathbf{r}, t) \rangle = 0,$$

$$\langle \eta_0(\mathbf{r}, t) \eta_0(\mathbf{r}', t') \rangle = 2k_B T \Gamma \delta(\mathbf{r} - \mathbf{r}') \delta(t - t'). \quad (3)$$

Theoretical solutions to Eq. (1) and experiments for the NCOP [20,21] show that the average domain or droplet size  $R$  increases as a function of time  $t$  like

$$R(t) \sim t^{1/2}. \quad (4)$$

The structure factor  $S(k, t)$  is the Fourier transform of the order parameter correlation function  $C(\mathbf{r}, t) = \langle \psi(\mathbf{r}, t) \psi(0, t) \rangle$ , where  $\psi(\mathbf{r}, t)$  is the local order parameter, and

$$\begin{aligned} S(\mathbf{k}, t) &= \langle \psi(\mathbf{k}, t) \psi(-\mathbf{k}, t) \rangle \\ &= R(t)^d \tilde{S}(kR(t)) \end{aligned} \quad (5)$$

in  $d$  dimensions, where  $k$  is a wave number and  $\tilde{S}(kR(t))$  is a scaling function. Note that for the NCOP one can define a characteristic length scale  $r_0$  where  $C(r_0, t) = C(0, t)/2$  [22], or the mean square domain size can be simply defined as

$$R^2(t) = \left\langle \frac{1}{N} \left[ \sum_{\mathbf{r}} \psi(\mathbf{r}, t) \right]^2 \right\rangle, \quad (6)$$

with total number of particles,  $N$ , which corresponds to the  $k=0$  peak of  $S(\mathbf{k}, t)$ , i.e.,  $S(0, t)$  [23].

### B. Surface roughening

The surface roughening of the nonequilibrium growth of thin films is usually characterized by the mean square fluctuation

$$w^2(t) = \langle (h(\mathbf{r}, t) - \langle h(t) \rangle)^2 \rangle, \quad (7)$$

where  $h(\mathbf{r}, t)$  is the height at lateral position  $\mathbf{r}$  and time  $t$  and  $\langle h(t) \rangle = (1/L^2) \sum_{\mathbf{r}} h(\mathbf{r}, t)$  with a lateral system size  $L$ . The mean square fluctuation has a scaling form

$$w^2(L, t) \sim L^{2\zeta} \tilde{f}(\xi(t)/L), \quad (8)$$

where  $\zeta$  is the roughness exponent and  $\xi(t) \sim t^{1/z}$  is the lateral correlation length which is described by the dynamic exponent  $z$ . The scaling function  $\tilde{f}(x) \sim x^{2\zeta}$  for  $x \ll 1$  and approaches a constant for  $x \gg 1$ . The structure factor

$$S_r(\mathbf{k}, t) = \langle \hat{h}(\mathbf{k}, t) \hat{h}(-\mathbf{k}, t) \rangle, \quad (9)$$

with  $\hat{h}(\mathbf{k}, t) = (1/L) \sum_{\mathbf{r}} [h(\mathbf{r}, t) - \langle h \rangle] e^{-i\mathbf{k} \cdot \mathbf{r}}$ , has a scaling form in the long-wavelength limit

$$S_r(\mathbf{k}, t) = k^{-\gamma} f(k^z t), \quad (10)$$

with  $\gamma = 2\zeta + d'$ , where  $d'$  is the substrate dimension. The scaling function  $f(x) \sim \text{const}$  for  $x \gg 1$  and, in the case of  $x \ll 1$ ,  $f(x) \sim x$  for  $\gamma \geq z$  and  $f(x) \sim x^{\gamma/z}$  for  $\gamma \leq z$  [24]. The dynamic exponent  $z$  can be determined from data collapse onto the scaling function

$$f(k^z t) = k^\gamma S_r(\mathbf{k}, t). \quad (11)$$

The continuum Langevin equation with conservation of the total number of particles is described in terms of surface diffusion current  $\mathbf{j}(\mathbf{r}, t)$  and nonconserved random noise  $\eta(\mathbf{r}, t)$ :

$$\frac{\partial h(\mathbf{r}, t)}{\partial t} = -\nabla \cdot \mathbf{j}(\mathbf{r}, t) + \eta(\mathbf{r}, t), \quad (12)$$

where the noise is assumed to satisfy  $\langle \eta(\mathbf{r}, t) \rangle = 0$  and  $\langle \eta(\mathbf{r}, t) \eta(\mathbf{r}', t') \rangle = 2D \delta^{d'}(\mathbf{r} - \mathbf{r}') \delta(t - t')$  with the diffusion coefficient  $D$ . If  $\mathbf{j} = -\nu \nabla h$ , one obtains a linear Langevin equation  $\partial h / \partial t = \nu \nabla^2 h + \eta$ , which has been solved exactly [18] and yields  $\zeta = 0$  and  $z = 2$  in  $d' = 2$ . It has been suggested that the hyperscaling relation [25]

$$z = 2\zeta + d' \quad (13)$$

holds for any growth model described by Eq. (12).

### III. MODEL AND METHOD

The simplest situation in heteroepitaxial film growth is when two different species ( $A$  and  $B$ ) are present and  $A$ -type material grows on a substrate of material  $B$  as in the growth of Ge on a Si substrate. Depending on the interfacial free energies and the lattice mismatch between the substrate and incoming particles, there are three possible modes of heteroepitaxial growth [26]: Frank-van der Merwe (FM), Volmer-Weber (VW), and Stranski-Krastanov (SK). However, here we neglect the effect of the lattice mismatch to simplify our model, so that the morphology of a growing film is entirely determined by the interfacial free energies.

In molecular-beam epitaxy, particles are randomly deposited at a given rate ( $F$ ), in units of monolayers per second (ML/s), on an initially flat substrate maintained with a fixed temperature ( $T$ ), and then diffuse around the surface or evaporate from the surface. In our MBE simulations, we consider a simple solid-on-solid model in which the substrate is a  $L \times L$  square lattice with periodic boundary conditions. Vacancies and overhangs are not allowed. Evaporation from the

surface is prohibited by assuming that our epitaxial temperature is not high enough for such evaporation. The deposition rate of  $A$ -type particles is  $xF$ , while for  $B$  it is  $(1-x)F$ , where  $x$  is the concentration of  $A$  particles. We have used an  $A$ -type substrate to mimic the growth of  $\text{Si}_{1-x}\text{Ge}_x$  on Si and deposited  $A$  and  $B$  particles with equal probability; i.e., we restrict ourselves to  $x=0.5$ .

A particle is randomly chosen for diffusion with an attempt frequency ( $D_0=80/\text{site s}$ ) after random deposition of  $A$  and  $B$  particles according to flux  $F$  and concentration  $x$ . Each particle can diffuse on the surface with probability  $P$ . We consider the hopping probability of breaking bonds between nearest-neighbor sites. The hopping probability ( $P_H$ ) is given by

$$P_H = \exp[-E(A,B)/k_B T], \quad (14)$$

where a site-dependent activation energy  $E(A,B)$  is determined by the local configurations of bonding between the nearest neighbors, i.e.,  $E(A,B) = n_{AA}J_{AA} + n_{BB}J_{BB} + n_{AB}J_{AB}$ , where  $n_{AA}$ ,  $n_{BB}$ , and  $n_{AB}$  are the number of  $A$ - $A$ ,  $B$ - $B$ , and  $A$ - $B$  pairs with nearest neighbors, respectively.  $J_{AA}$ ,  $J_{BB}$ , and  $J_{AB}$  are effective bond energies between  $A$ - $A$ ,  $B$ - $B$ , and  $A$ - $B$  with  $(J_{AA}, J_{BB}, J_{AB}) = (-J, -J, J)$ , and  $J > 0$ . An  $A$ -( $B$ -) type particle tends to make a bond with a  $B$ -( $A$ -) type particle due to ‘‘antiferromagnetic-like’’ effective interactions.

After breaking the bonds, a particle at the  $i$ th site diffuses to a nearest-neighbor  $k$ th site with probability

$$P_D(i \rightarrow k) = \exp[-E_k(A,B)/k_B T], \quad (15)$$

where  $E_k(A,B)$  is the binding energy available at the  $k$ th site, and particles hop up no more than one lattice constant. The hop is carried out depending on the magnitude of a random number (RN) generated such that  $0 < \text{RN} < \sum P_D$ , which is proportional to the probability of hopping to the site. Therefore a particle prefers to move to a site which provides the greatest binding energy. The homoepitaxial version of this method has been used in other papers [27]. By using this simulational model and method for binary alloy film growth, we hope to capture the essential features of the nonequilibrium behavior of domain growth and surface roughening; however, we do not expect this simple model to provide a quantitative description of a physical alloy film.

Simulations have been carried out for  $20 \leq L \leq 200$  with the different number of layers grown depending on the system size  $L$  using IBM RS6000 and Pentium workstations. The growth is repeated with different random number and results are averaged to reduce the statistical errors; for example, 800 different runs have been averaged for  $L=80$ . We have used a uniform random number generator based on the linear congruential method [28]. All the length scales have been measured in the unit of a lattice constant  $a$ , e.g., system size  $L \equiv L/a$ .

To see the evolution of the LRO and the domain size, we have relied on a lattice gas model for a binary alloy. The model can be described in terms of a spin-1 Ising model [29]. If the  $\mathbf{r}$  site at a layer number  $l$  is occupied by an  $A$  ( $B$ ) atom at time  $t$ , then  $\sigma(\mathbf{r}, l) = 1$  ( $-1$ ). Otherwise, the site is empty and  $\sigma(\mathbf{r}, l) = 0$ . There are many spin updatings due to the deposition and diffusion; so all the spin configurations

inside the bulk must be recorded. After the LRO reaches its asymptotic value, we have turned off the flux and quenched the system. The quenched order and the mean square quenched order are defined as

$$M(l) = \left\langle \left[ \frac{1}{N} \sum_{\mathbf{r}} (-1)^{\mathbf{r}} \sigma(\mathbf{r}, l) \right] \right\rangle, \quad (16)$$

$$M^2(l) = \left\langle \left[ \frac{1}{N} \sum_{\mathbf{r}} (-1)^{\mathbf{r}} \sigma(\mathbf{r}, l) \right]^2 \right\rangle, \quad (17)$$

where  $N=L^2$  and  $\sigma(\mathbf{r}, l)$  can be 1 (or  $-1$ ) if an  $A$  (or  $B$ ) atom occupies the site because of the assumption of no overhang and no vacancy. The quenched order  $M(l)$  has been calculated up to the maximum layer number  $l_m$  for which the layer is entirely filled.

Since we assume that bulk diffusion is negligible, all the past history of the surface, LRO and SRO fluctuations, along the growth direction [001] and in each layer are recorded in the bulk. The height-height and atom-atom correlations increase as films grow and finally saturate after the deposition of certain number of layers in a finite size system. In that sense, one may regard the layer number  $l$  as time, and thus the domain size at the layer number  $l$  may be defined as the  $k=0$  peak of structure factor  $S(\mathbf{k}, l)$ , i.e.,  $S(0, l)$ . The structure factor is defined as

$$S(\mathbf{k}, l) = \frac{1}{N} \sum_{\mathbf{r}, \mathbf{r}'} \exp[i\mathbf{k} \cdot (\mathbf{r} - \mathbf{r}')] \langle \psi(\mathbf{r}, l) \psi(\mathbf{r}', l) \rangle, \quad (18)$$

where  $\psi(\mathbf{r}, l) = (-1)^{\mathbf{r}} \sigma(\mathbf{r}, l)$ . In analogy to Eq. (6), we define the mean square domain size as

$$R^2(l) = NM^2(l). \quad (19)$$

The domain size  $R(l)$  is also related to the domain growth exponent  $z_R$  at late times,

$$R(l) \sim l^{1/z_R}, \quad (20)$$

based on the self-similar behavior of the domain growth.

## IV. RESULTS

### A. Results for domain growth

The results of domain growth of our model are consistent with Allen-Cahn theory [30] for the NCOP. According to the theory, the normal velocity of a curved antiphase boundary (APB) is linearly proportional to the mean curvature. The motion of the APB evolves in such a way as to reduce the curvature in order to minimize surface tension by bulk diffusion. In the case of domain growth by MBE, the pattern of ordered domains and antiphase boundaries at early time affects the morphology of growing films and the average size of ordered clusters. The layer number dependence of the motion of the APB shows nontrivial behavior due to the surface roughening and competition between ordering and disordering by thermal fluctuations.

Figure 1 shows a series of snapshots of ordered domains and antiphase boundaries in four different layers. The first layer, shown in Fig. 1(a), is relatively disordered com-

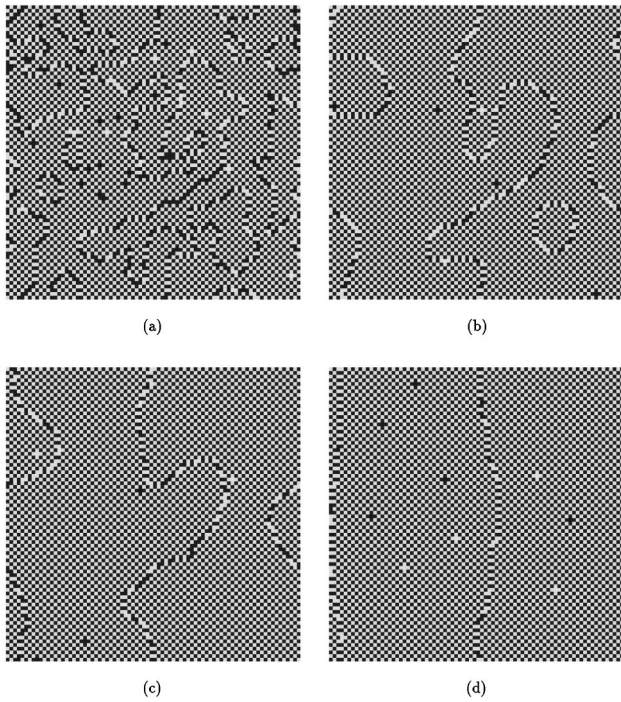


FIG. 1. A series of snapshots of ordered domains and antiphase boundaries in four different layers  $l=1$  (a), 50 (b), 100 (c), and 600 (d) for a system size  $L=80$ ,  $k_B T/J=1.0$ , and a deposition rate  $F=1$  ML/s. A white (black) square is an  $A$  ( $B$ ) adatom in the layer.

pared to other layers, due in large part to the homogeneous  $A$ -type substrate. The density of APB's near the substrate is much larger than near the surface. As  $l$  becomes large, the APB's straighten out or even disappear, and finally the system reaches its steady state after a layer number  $l_s$  at which LRO saturates. It is worth noting that the circular APB's seen in Fig. 1(b) are eliminated in Fig. 1(c) by the coarsening kinetics.

As illustrated in Fig. 1, a partially ordered layer acts as a template for further ordering in the next layer. At early stages, small ordered clusters are formed by energy density

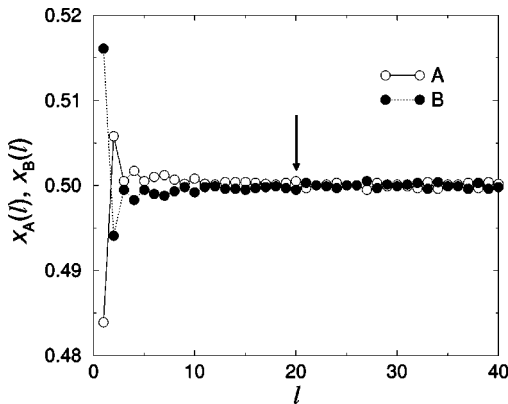


FIG. 2. Layer dependence of the concentrations  $x$  of  $A$  and  $B$  adatoms for quenched films after the deposition of 100 layers for  $L=80$ ,  $k_B T/J=1.0$ , and  $F=1$  ML/s: the concentrations  $x$  of  $A$  and  $B$  adatoms in a layer number  $l$  are defined as  $x_A(l) = (1/2N) \sum_r [\sigma(r, l) + 1]$  and  $x_B(l) = 1 - x_A(l)$ . Errors in the individual points are smaller than the symbol size.

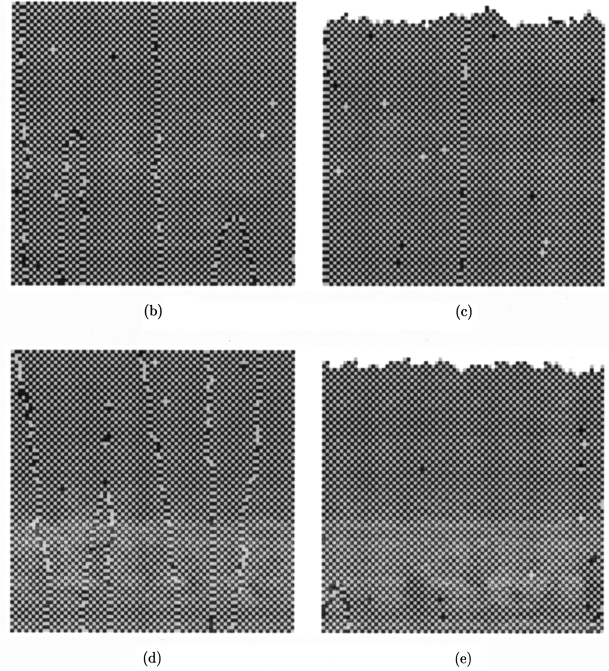
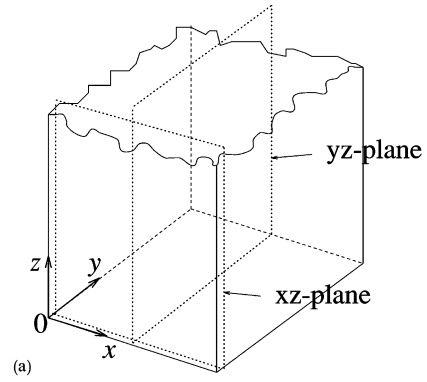


FIG. 3. Illustration of two planes and vertical cross sections of a film after deposition of 800 layers for  $L=80$ ,  $k_B T/J=1.0$ , and  $F=1$  ML/s. (a) Illustration of two planes for  $L=80$  used for (b)–(e). (b)  $xz$  plane showing the first 80 layers. (c)  $xz$  plane showing  $724 \leq l \leq 805$ . (d)  $yz$  plane showing the first 80 layers. (e)  $yz$  plane showing  $724 \leq l \leq 805$ . A white (black) square is an  $A$  ( $B$ ) adatom in the layer.

fluctuations, i.e., SRO fluctuations [31], which develop LRO domains and begin to coalesce and finally fill the first layer as the film grows. The nucleation of small ordered clusters may occur on top of the growing domains, so that an ordered layer produces more ordering in the next layer. This behavior is consistent with the results of kinetic mean field theory [16].

At this stage, the nonlinear term  $(\kappa_0/2)(\nabla\psi)^2$  in the free energy density described in Eq. (2) is large and  $V(\psi) \approx \frac{1}{2}r_0\psi^2$  for a large system size  $L$ . The effect of the substrate and the strong nonlinear term lead to a transient behavior up to  $l \approx 20$ . We can clearly see the transient behavior in Fig. 2 showing the concentration  $x$  of  $A$  and  $B$  adatoms as a function of layer number  $l$ . The density of  $B$  adatoms in the first layer is a little larger than that of  $A$  adatoms; however, it oscillates around 0.5 as the film grows because the total number of particles is conserved; i.e.,  $x_A$  and  $x_B$  of adatoms

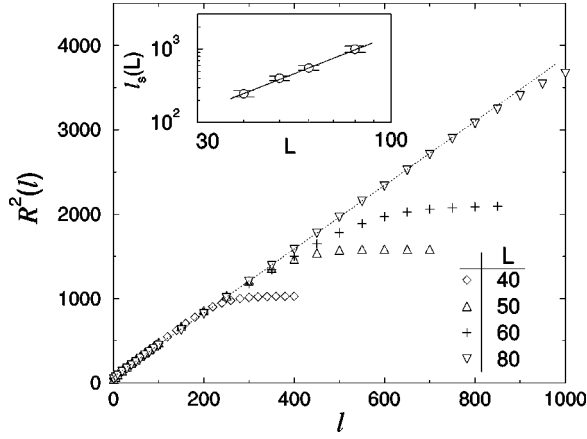


FIG. 4. Mean square domain size  $R^2(l)$  as a function of the layer number  $l$  for  $40 \leq L \leq 80$ ,  $k_B T/J = 1.0$ , and  $F = 1$  ML/s. Errors in the individual points are comparable to the symbol size. The dotted line is a linear fit,  $R^2(l) = R^2(0) + A(T)l$ , with  $R^2(0) = 17.1$ , and the rate constant  $A = 3.78$ . The inset shows the saturation of  $R^2(l)$  after the layer number  $l_s(L)$  as a function of  $L$ . The solid line in the inset is a power-law fit  $l_s(L) \sim L^{z_R}$ , with the dynamic exponent  $z_R = 2.02$

deposited at each time step are the same. After the transient behavior ( $l \geq 20$ ) indicated by the arrow,  $x_A(l) \approx x_B(l)$ , i.e.,  $(1/N) \sum_r \sigma(\mathbf{r}, l) \approx 0$  in each layer.

Figures 3(b)–3(e) show vertical cross sections of films after deposition of 800 layers. Figures 3(b) and 3(d) are the sections for  $1 \leq l \leq 80$  along the  $xz$ - and  $yz$  planes illustrated in Fig. 3(a), respectively. The rough surface can be seen in Figs. 3(c) and 3(e) in both planes. As shown in Figs. 3(b) and 3(c), the ordered domain size grow and the streaks of APB's extend vertically from the substrate to the surface. Some of the APB's are eliminated by the coarsening process. Unlike the curved APB's in a plane perpendicular to the growth direction shown in Figs. 1(a), 1(b), and 1(c), the shape of APB's along the growth directions is almost linear. These are in good agreement with experiments [6,7,9] and simulations of CuPt type of ordering [32,33].

Figure 4 shows the mean square domain size  $R^2(l)$  as a function of a layer number  $l$  for  $40 \leq L \leq 80$ . The dotted line in Fig. 4 is a linear fit for  $L = 80$  after the initial transient behavior ( $l \geq 20$ )

$$R^2(l) = R^2(0) + A(T)l, \quad (21)$$

where  $A(T)$  is a temperature-dependent rate constant. The linear behavior of  $R^2(l)$  agrees very well with the results of a NCOP domain coarsening by order-disorder phase transitions [12,30] if one regards  $l$  as time  $t$ . Here  $R^2(l)$  saturates after  $l_s(L)$  due to finite size effects and the inset in Fig. 4 shows that  $l_s(L) \sim L^{z_R}$  with domain growth exponent  $z_R = 2.02 \pm 0.30$ , where we have used  $L \geq 40$  for the power-law fit. For large  $l$ , Eq. (21) can be approximated by

$$R(l) \approx \sqrt{A(T)} l^{1/2} \left( 1 + \frac{R^2(0)}{2A(T)l} \right). \quad (22)$$

Equation (22) indicates that for large  $L$  and  $l$ ,  $R(l) \sim l^{1/2}$  similar to Eq. (4),  $R(t) \sim t^{1/2}$  for the NCOP domain growth.

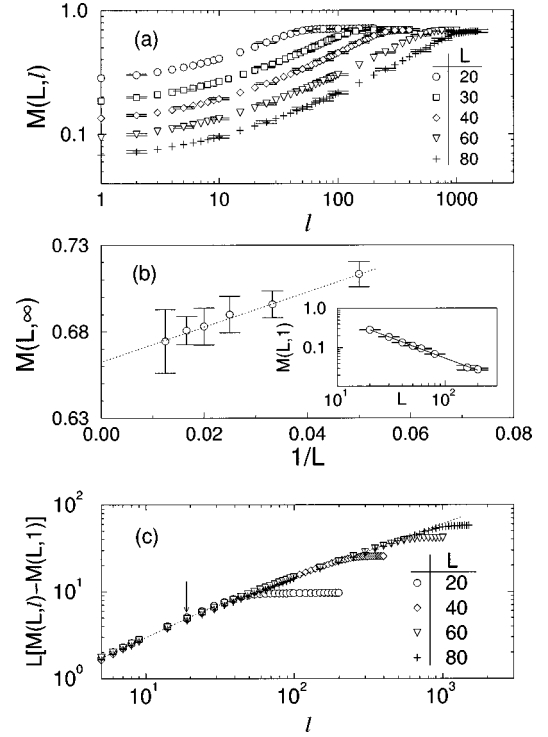


FIG. 5. (a) The long-range order parameter  $M(L, l)$  as a function of the layer number  $l$  for  $20 \leq L \leq 80$ ,  $k_B T/J = 1.0$ , and  $F = 1$  ML/s. (b) The saturated LRO  $M(L, \infty)$  as a function of the inverse system size  $1/L$ . In the thermodynamic limit,  $M(L \rightarrow \infty, \infty) \approx 0.663 \pm 0.015$  for  $k_B T/J = 1.0$  and  $F = 1$  ML/s. The inset in (b) shows LRO at the layer number  $l = 1$ . The solid line in the inset is a power-law fit  $M(L, 1) \sim L^{-1.03 \pm 0.05}$  for  $20 \leq L \leq 200$ . (c) A quantity  $L[M(L, l) - M(L, 1)]$  as a function of  $l$  for the same parameters as above. The transient behavior persists up to the layer indicated by the arrow. (c) indirectly implies that  $R^2(l)$  is a correct scaling quantity.

The exponent  $z_R$  obtained agrees well with the asymptotic behavior of  $R(l)$  given in Eq. (22).

Figure 5(a) explains the behavior of the LRO as a function of  $l$ . We have also found that the LRO depends sensitively on epitaxial parameters like deposition conditions and intrinsic properties like activation energies. Figure 5(b) shows the steady-state nonequilibrium LRO ( $M_{ne}$ ) as a function of  $1/L$ . In the thermodynamic limit,  $M(L \rightarrow \infty, \infty) \approx 0.663$  and the LRO in the first layer,  $M(L, 1) \sim L^{-1.03}$ , as shown in the inset of Fig. 5(b). Note that the equilibrium LRO ( $M_{eq}$ ) of the two-dimensional Ising model is approximately 0.98 for  $k_B T/J = 1.0$ . The discrepancy between  $M_{eq}$  and  $M_{ne}$  may result from the intrinsic nonequilibrium behavior of growth by MBE. Figure 5(c) indirectly implies that  $R^2(l)$  is a correct scaling quantity. As the film grows, the surface becomes rough and the saturated interfacial width  $w_s$  diverges so that the surface roughening is closely related to the magnitude of the LRO. From the results of  $M(L, \infty)$  and  $M(L, 1)$ , we have obtained  $M(L, \infty) - M(L, 1) = a - b/L$  with  $a = 0.663$  and  $b = 4.57$ .

## B. Temperature dependence of the domain size

In Fig. 6 we have compared the relaxation kinetics of  $S(0, l)$  for two different ranges of  $T$ ,  $0.5 \leq k_B T/J \leq 2.0$  and  $3.85 \leq k_B T/J \leq 4$ . The temperature dependence of  $R^2(t)$  in

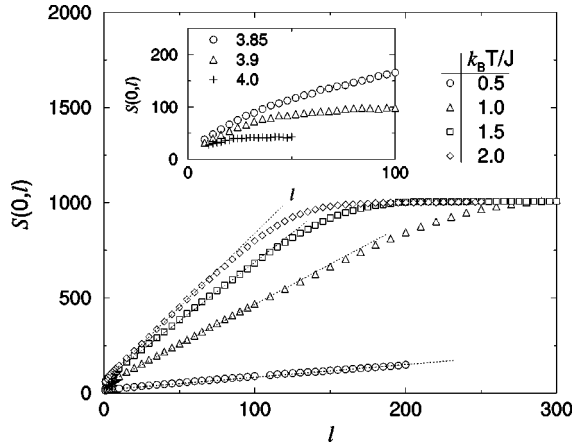


FIG. 6. Temperature dependence of the structure factor  $S(0,l)$  for  $L=40$ ,  $0.5 \leq k_B T/J \leq 2.0$ , and  $F=1$  ML/s. The dotted lines are linear fits after the layer number  $l \geq 20$ . The inset shows  $S(0,l)$  at high temperatures,  $k_B T/J=3.85$ ,  $3.9$ , and  $4.0$  for  $L=40$  and  $F=1$  ML/s. Errors in the individual points are comparable to the symbol size.

order-disorder phase transitions can be obtained from  $R^2(T,t) = S(0,t)/\psi_{\text{eq}}^2(T)$  [23], where  $\psi_{\text{eq}}(T)$  is the equilibrium value of LRO. Because of the practical difficulties of defining  $\psi_{\text{eq}}(T)$ , we simply plotted  $S(0,l)$  as a function of  $l$  instead of  $R^2(l)$ . The dotted lines in Fig. 6 are linear fits to data for  $l \geq 20$ , i.e., after the transient behavior. A slow relaxation of LRO toward a steady state occurs at low temperature in contrast to a fast relaxation at high temperature. However, the slope of the dotted line, defined as  $B(T)$ , at  $k_B T/J=3.85$  is smaller than that at  $k_B T/J=2.0$ . This result indicates the presence of a maximum slope at temperature  $T_m$ . Note that the saturation value of  $S(0,l)$  at  $k_B T/J=2.0$  is approximately 10 times as great as that of  $S(0,l)$  at  $k_B T/J=3.9$ .

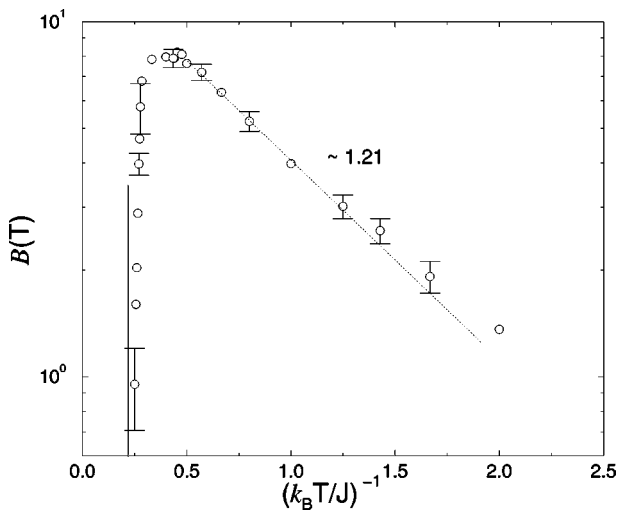


FIG. 7. The temperature dependence of the slope  $B(T)$  for  $L=40$ ,  $0.5 \leq k_B T/J \leq 3.65$ , and  $F=1$  ML/s. The dotted line is a least-squares fit with  $B(T) \sim \exp(-s/k_B T)$  and  $s \sim 1.21J$  for temperature range  $0.6 \leq k_B T/J \leq 2.2$ . The vertical line is at the inverse critical temperature of the three-dimensional simple cubic Ising model [ $k_B T_c(3D)/J \approx 4.510$ ].

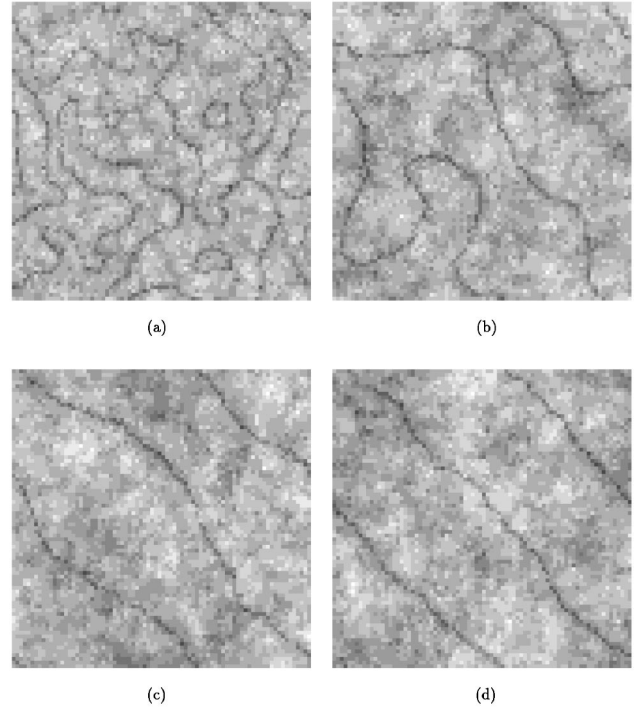


FIG. 8. A series of top views of surfaces of growing films at four different time  $t=10$  (a),  $100$  (b),  $500$  (c), and  $2000$  (d) for  $L=80$ ,  $k_B T/J=1$ , and  $F=1$  ML/s. The interfacial width  $w(L,t)$  saturates approximately after time  $t=1200$  for  $L=80$ . A lighter color represents a higher height compared to a dark color for a lower height.

As the temperature increases, the saturated value of the LRO decreases, and finally converges to a finite nonzero value due to finite size effects. These can be understood in terms of thermal competition between mobility and spontaneous ordering. Another important factor which we need to consider is the temperature dependence of surface roughening. Experiments show that at low temperatures the surface of a growing film becomes rough indicating high surface free energy. For higher flux, the lack of diffusion makes the surface rough and produces less ordering inside the film [9]. We have also observed less ordering for high flux. This result suggests that the decrease in surface diffusion length makes it difficult for adatoms to overcome energy barriers and hop over the rough surface to find a locally stable state to form an ordered cluster.

Figure 7 shows the temperature dependence of  $B(T)$  for  $0.5 \leq k_B T/J \leq 4$ . It is difficult to measure the  $B(T)$  for  $k_B T/J > 4.0$  due to the very fast relaxation. The vertical line in Fig. 7 is at the inverse critical temperature [ $T_c(3D)$ ] of the three-dimensional simple-cubic Ising model. The slope  $B(T)$  shows a simple Arrhenius behavior  $\exp(-s/k_B T)$ , with  $s = 1.21J$  for  $0.8 \leq k_B T/J \leq 2.2$ . At low temperature, the process may not reach the region of the domain coarsening driven by the interfacial free energy.  $B(T)$  has a maximum at  $k_B T_m/J \approx 2.2$ , and there is no significant change in  $B(T)$  for temperatures between  $2.1$  and  $2.4$ . As the temperature increases above  $k_B T/J=3.0$  and approaches  $T_c(3D)$ , a sharp decrease in  $B(T)$  occurs. The results imply that the kinetics of the domain growth in this model is indeed a three-dimensional process.

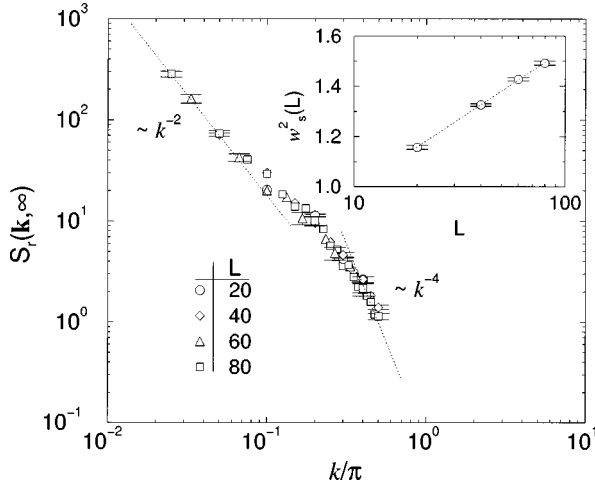


FIG. 9. The steady-state structure factor  $S_r(\mathbf{k}, \infty)$  as a function of wave number  $k$  for  $k_B T/J=1.0$  and  $F=1$  ML/s. In long-wavelength limit,  $S_r(\mathbf{k}, \infty) \sim k^{-2}$ , and for large  $k$  modes, there is a crossover to  $\gamma=4$ . The inset shows that the saturated mean square width  $w_s^2(L) \sim \ln(L)$  and implies  $\zeta=0$ .

### C. Results for surface roughening

In Fig. 8 we show the effect of kinetic ordering and APB's on the surface roughening. Curved dark lines indicate lower height and imply the presence of APB's on the surface. The growth of films around the dark lines is relatively suppressed because of the high surface free energy of the APB, so that ordering and relatively higher heights are found between the APB's. Since the saturation time  $\tau$  of  $w(L, t)$  is slightly larger than that of domain growth, the number and shapes of APB's on the surface do not change even after the saturation of the interfacial width  $w(L, t)$ . Those results imply that the kinetic ordering and the motion of APB's are coupled to the surface roughening during growth.

Since the mean square width  $w^2(t) = (1/L^2) \sum_{\mathbf{k}} S_r(\mathbf{k}, t)$ ,  $w(t)$  contains less information than the structure factor  $S_r(\mathbf{k}, t)$  itself [24]. Thus more detailed information of growing films can be obtained from the structure factor. For small  $k$  modes and correlation length  $\xi(t) < 1/k$ , the growth of  $S_r(\mathbf{k}, t) \sim t$  is uncorrelated with other modes. As the film grows, the correlation length  $\xi(t)$  becomes larger and finally  $S_r(\mathbf{k}, t)$  saturates after  $k > 1/\xi(t)$ . The divergence of  $S_r(\mathbf{k}, t)$  in the long-wavelength limit is responsible for that of  $w^2(t)$  when  $L \rightarrow \infty$ . Figure 9 shows that the steady-state structure factor  $S_r(\mathbf{k}, \infty) \sim k^{-\gamma}$  with  $\gamma=2$  in the long-wavelength limit and the saturated mean square interfacial width  $w_s^2(L) \sim \ln(L)$ , implying  $\zeta=0$ . For large  $k$  modes, it seems that there is a crossover to  $\gamma=4$ , meaning that surface diffusion is the main relaxation process at small length scales [25,34]. The behavior of  $w_s^2(L)$  agrees with the experimental results of surface roughening in  $\text{Si}_{1-x}\text{Ge}_x$  film growth on Si at large length scales [17]. The dynamic exponent  $z=2.00 \pm 0.15$  is obtained from the data collapse onto the scaling function  $f(k^z t)$  in Eq. (11) for several  $k$  modes shown in Fig. 10.

The exponents obtained obey the hyperscaling relation  $z=2\zeta+d'$  [25] and indicate the growth exponent  $\zeta/z=0$  at late stages. However, we have difficulty obtaining  $\zeta/z$  directly from  $w(t)$  due to the initial transient behavior. Simulations using a much larger system size  $L$  are needed to con-

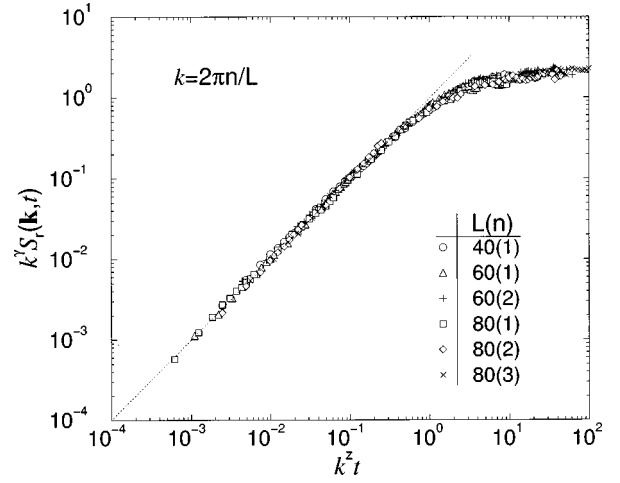


FIG. 10. The scaling function  $f(k^z t) = k^\gamma S_r(\mathbf{k}, t)$  as a function of the scaled time  $k^z t$  with  $\gamma=z=2.0$  for several  $k$  modes,  $k_B T/J=1.0$ , and  $F=1$  ML/s. The dotted line is a guide line with slope = 1.

firm the result, and this would require a huge amount of computer resources. A detailed error analysis [35] shows that the error in  $f(k^z t)$ ,

$$\sigma_f \approx \frac{S_r(\mathbf{k}, t)}{S_r(\mathbf{k}, \infty)} \left[ \left( \frac{\sigma_t}{S_r(\mathbf{k}, t)} \right)^2 + \left( \frac{\sigma_\infty}{S_r(\mathbf{k}, \infty)} \right)^2 \right]^{1/2},$$

if  $S_r(\mathbf{k}, t)$  is uncorrelated with  $S_r(\mathbf{k}, \infty)$ , and the error in the scaled time  $\tau = k^z t$ ,  $\sigma_\tau \approx |\ln(k)| \sigma_z k^z t$ , where  $\sigma_t$ ,  $\sigma_\infty$ , and  $\sigma_z$  are errors in  $S_r(\mathbf{k}, t)$ ,  $S_r(\mathbf{k}, \infty)$ , and  $z$ , respectively.

The continuum growth equation which can describe the kinetic roughening of our model [36] at late stages is given by

$$\frac{\partial h}{\partial t} = \nu \nabla^2 h - \kappa \nabla^4 h + \eta(\mathbf{r}, t). \quad (23)$$

Here  $\nu \nabla^2 h$  in Eq. (23) is a Laplacian (EW) term and  $\kappa \nabla^4 h$  is related to the surface diffusion. As a test of whether a nonlinear term is present or not, we have calculated the skewness which is defined as  $S_3(t) = \langle (h - \langle h \rangle)^3 \rangle / \langle (h - \langle h \rangle)^2 \rangle^{3/2}$ . Nonzero skewness implies that up-down symmetry is broken and a nonlinear term is present. We have obtained the skewness  $S_3 = -0.06 \pm 0.01$  for  $L=80$  in the asymptotic regime, meaning that the magnitude of the nonlinear term is very small. Our data show that the skewness becomes smaller with increasing substrate size  $L$ , and we believe that it is likely to be zero for  $L=\infty$ . If this is correct, then the presence of any nonlinear term in Eq. (23) is excluded in an asymptotic growth equation.

The Laplacian term in Eq. (23) dominates at large length scales and determines the final morphology of films in contrast to that at small length scales, where the surface diffusion term dominates, leading to  $w_s^2(L) \sim L^2$ . The above Langevin equation without the nonlinear Kardar-Parisi-Zhang (KPZ) term  $(\lambda/2)(\nabla h)^2$  [37] may also explain the surface roughening in  $\text{Si}_{1-x}\text{Ge}_x$  film growth on Si [17]; however, the skewness actually found for Si-Ge films is nonzero, which may arise from the desorption or vacancies (overhangs) at late times. The asymptotic behavior of  $w_s^2(L)$  shown in Fig. 9 is consistent with the above theoretical de-

scription in which the final stage of surface morphology is determined by the EW term, leading to the scaling behavior  $w_s^2(L) \approx (D/2\pi\nu)\ln(L)$  [18,38].

At this moment, theoretical continuum equations available for the growth by MBE are based on homoepitaxial film growth. Thus the effect of substrate and inhomogeneous interactions between different kinds of particles on the surface roughening is less clear. Further studies are needed to produce a better understanding of the binary mixture film growth.

## V. CONCLUSION

In this paper we have considered multilayer  $A_{0.5}B_{0.5}$  film growth on  $A[001]$  by molecular-beam epitaxy simulations. This study encompassed both growth-induced domain coarsening and noise-induced surface roughening. Our model includes the essential feature of molecular-beam epitaxy; i.e., we have adopted the random deposition of particles and surface diffusion.

The antiphase boundaries initially induced by the substrate and the random deposition of a binary mixture are eliminated by the coarsening process, leading to a large ordered domain as films grow when bulk diffusion is negli-

gible. Since the magnitude of the long-range order increases as the layer number increases, our results for the domain growth are similar to that of the case of a nonconserved order parameter. The temperature dependence of the peak of the structure factor shows that the domain growth is indeed a three-dimensional process. There is a temperature that results in a maximum of the peak because of the competition between the mobility and spontaneous ordering. Because of the surface roughening, we find less ordering compared to the case of the two-dimensional Ising model.

The presence of the antiphase boundaries on the surface indicates a correlation between the domain growth and the surface roughening. The Laplacian term in the continuum growth equation determines the final morphology of films in the asymptotic regime. More extensive studies are needed to understand the coupling between growth-induced pattern formation and surface roughening.

## ACKNOWLEDGMENTS

We thank F. Family and A. Zangwill for helpful discussions. The work was supported by the National Science Foundation under Grant No. DMR-9727714 at the University of Georgia.

- 
- [1] *Molecular Beam Epitaxy Application to Key Materials*, edited by Robin F. C. Farrow (Noyes Publications, Park Ridge, NJ, 1995) and references therein.
- [2] F. Family and T. Vicsek, *Dynamics of Fractal Surfaces* (World Scientific, Singapore, 1991); A.-L. Barabasi and H. E. Stanley, *Fractal Concepts in Surface Growth* (Cambridge University Press, Cambridge, England, 1995) and references therein.
- [3] F. K. LeGoues, V. P. Kesan, and S. S. Iyer, Phys. Rev. Lett. **64**, 40 (1990); V. P. Kesan, F. K. LeGoues, and S. S. Iyer, Phys. Rev. B **46**, 1576 (1992).
- [4] T. S. Kuan, T. F. Kuech, W. I. Wang, and E. L. Wilkie, Phys. Rev. Lett. **54**, 201 (1985).
- [5] B. A. Philips, I. Kamiya, K. Hingerl, L. T. Florez, D. E. Aspnes, S. Mahajan, and J. P. Harbison, Phys. Rev. Lett. **74**, 3640 (1995); M. A. Shahid, S. Mahajan, D. E. Laughlin, and H. M. Cox, *ibid.* **58**, 2567 (1987).
- [6] P. Bellon, J. P. Chevalier, E. Augarde, J. P. Andre, and G. P. Martin, J. Appl. Phys. **66**, 2388 (1989).
- [7] A. Gomyo, T. Suzuki, and S. Iijima, Phys. Rev. Lett. **60**, 2645 (1988).
- [8] A. Ourmazd and J. C. Bean, Phys. Rev. Lett. **55**, 765 (1985); F. K. LeGoues, V. P. Kesan, S. S. Iyer, J. Tersoff, and R. Tromp, *ibid.* **64**, 2038 (1990).
- [9] D. S. Cao, A. W. Kimball, G. S. Chen, K. L. Fry, and G. B. Stringfellow, J. Appl. Phys. **66**, 5384 (1989); D. S. Cao, E. H. Reihlen, G. S. Chen, A. W. Kimball, and G. B. Stringfellow, J. Cryst. Growth **109**, 279 (1991).
- [10] N. Ikarashi, K. Akimoto, T. Tatsumi, and K. Ishida, Phys. Rev. Lett. **72**, 3198 (1994).
- [11] E. G. McRae and R. A. Malic, Phys. Rev. Lett. **65**, 737 (1990).
- [12] B. Park, G. B. Stephenson, S. M. Allen, and K. F. Ludwig, Jr., Phys. Rev. Lett. **68**, 1742 (1992).
- [13] D. E. Jesson, S. J. Pennycook, J. Z. Tischler, J. D. Budai, J.-M. Baribeau, and D. C. Houghton, Phys. Rev. Lett. **70**, 2293 (1993).
- [14] G. B. Stringfellow, L. C. Su, Y. E. Strausser, and J. T. Thornton, Appl. Phys. Lett. **66**, 3155 (1995).
- [15] J. R. Smith, Jr. and A. Zangwill, Phys. Rev. Lett. **76**, 2097 (1996).
- [16] A. Zangwill, J. Cryst. Growth **163**, 8 (1996).
- [17] C.-Y. Mou and J. W. P. Hsu, Phys. Rev. B **53**, R7610 (1996).
- [18] S. F. Edwards and D. R. Wilkinson, Proc. R. Soc. London, Ser. A **381**, 17 (1982).
- [19] P. C. Hohenberg and B. I. Halperin, Rev. Mod. Phys. **49**, 435 (1977).
- [20] A. J. Bray, Adv. Phys. **43**, 357 (1994) and references therein.
- [21] G.-C. Wang and T.-M. Lu, Phys. Rev. Lett. **50**, 2014 (1983).
- [22] M. Siegert, in *Scale Invariance, Interface, and Non-equilibrium Dynamics*, edited by A. Mckane *et al.* (Plenum Press, New York, 1995), p. 165.
- [23] A. Sadiq and K. Binder, J. Stat. Phys. **35**, 517 (1984); E. T. Gawlinski, M. Grant, J. D. Gunton, and K. Kaski, Phys. Rev. B **31**, 281 (1985).
- [24] M. Siegert and M. Plischke, Phys. Rev. E **50**, 917 (1994).
- [25] D. F. Wolf and J. Villain, Europhys. Lett. **13**, 389 (1990).
- [26] D. J. Eaglesham and M. Cerullo, Phys. Rev. Lett. **64**, 1943 (1990).
- [27] S. Pal and D. P. Landau, Phys. Rev. B **49**, 10 597 (1994); D. P. Landau and S. Pal, Langmuir **12**, 29 (1996); Thin Solid Films **272**, 184 (1996).
- [28] I. Vattulainen, K. Kankaala, J. Saarinen, and T. Ala-Nissila, Comput. Phys. Commun. **86**, 209 (1995).
- [29] Y. Saito, J. Chem. Phys. **74**, 713 (1981); Y. Saito and H. Müller-Krumbhaar, *ibid.* **74**, 721 (1981).

- [30] S. M. Allen and J. W. Cahn, *Acta Metall.* **27**, 1085 (1979).
- [31] Y. Saito and R. Kubo, *J. Stat. Phys.* **15**, 233 (1976).
- [32] M. Ishimaru, S. Matsumura, N. Kuwano, and K. Oki, *Phys. Rev. B* **51**, 9707 (1995).
- [33] S. Matsumura, K. Takano, N. Kuwano, and K. Oki, *J. Cryst. Growth* **115**, 194 (1991).
- [34] J. M. Kim and S. Das Sarma, *Phys. Rev. Lett.* **72**, 2903 (1994).
- [35] P. R. Bevington, *Data Reduction and Error Analysis for the Physical Sciences* (McGraw-Hill, New York, 1969).
- [36] S. Das Sarma and S. V. Ghaisas, *Phys. Rev. Lett.* **69**, 3762 (1992).
- [37] M. Kardar, G. Parisi, and Y. C. Zhang, *Phys. Rev. Lett.* **56**, 889 (1986).
- [38] T. Nattermann and L.-H. Tang, *Phys. Rev. A* **45**, 7156 (1992).